

# Dynamic *in situ* observation of rapid size and shape change of supported Pd nanoparticles during CO/NO cycling

MARK A. NEWTON<sup>1\*</sup>, CAROLINA BELVER-COLDEIRA<sup>2</sup>, ARTURO MARTÍNEZ-ARIAS<sup>2</sup> AND MARCOS FERNÁNDEZ-GARCÍA<sup>2\*</sup>

<sup>1</sup>The European Synchrotron Radiation Facility, 6, Rue Jules Horowitz, BP-220, Grenoble, France

<sup>2</sup>Instituto de Catalisis y Petroleoquímica, CSIC, C/Marie Curie 2, 28049 Madrid, Spain

\*e-mail: newton@esrf.fr; mfg@icp.csic.es

Published online: 27 May 2007; doi:10.1038/nmat1924

**Understanding and improving the behaviour of supported precious-metal catalysts for a vast array of environmentally and economically important processes is a central area of research in catalysis. The removal of toxic gases such as CO and NO, without forming others (such as N<sub>2</sub>O), is particularly important. By combining energy-dispersive extended X-ray absorption fine-structure spectroscopy with a vibrational spectroscopy (infrared) and mass spectrometry, at high time resolution, in a single *in situ* experiment, we dynamically observe and quantify CO-, and subsequent NO-, induced size and shape changes of Pd nanoparticles during CO/NO cycling. In doing so we demonstrate a novel, non-oxidative redispersion (for example, an increase in metal surface area) mechanism, and suggest a model to bridge the structural and reactive functions of supported Pd catalysts.**

Supported catalysts based on precious metals, such as palladium, platinum and rhodium, are used in a vast array of processes of environmental, practical and economic importance. These range from the reforming and cracking of hydrocarbon feedstocks to the use of such catalysts in the abatement of noxious gas emissions from petrol- or diesel-driven engines. Associated with these applications are many reasons to improve catalyst performance, such as to protect the environment, minimize the use of such expensive metals—through lower loadings, increased catalyst longevity or recyclability—or to design catalysts that can work under ever more demanding process conditions.

A long-standing problem is the tendency of nanoscale particles of such elements to coalesce ('sinter') into much larger aggregates under process conditions<sup>1</sup>. This leads to deactivation of the catalyst caused by the reduction of the surface area of the precious metal available to the reactant species. In addition, the chemistry exhibited by these systems is often highly sensitive to the domain size of the active metal itself<sup>2</sup>. Therefore, sintering can also result in a catalyst exhibiting a different behaviour to that desired.

It is known that such sintering processes can be reversed, at least in part, through the application of high-temperature oxidation methods and subsequent re-reduction<sup>3–7</sup>. However, this is not a panacea and, to be effective, requires the presence of chlorine (Cl) either in the catalyst formulation or in the gas phase. Ideally, the use of Cl should be avoided entirely, both on environmental and practical grounds.

Although there has been considerable research into sintering and redispersion phenomena<sup>3–7</sup>, and adsorbate-induced morphological variation in metal nanoparticles, this has generally been limited to relatively static assessments of the systems under study; these range from the *ex situ* transmission electron microscopy (TEM) work of Harris<sup>8</sup> (refaceting of Pt particles after

exposure to H<sub>2</sub>S) to *in situ* TEM studies of shape change in Cu particles of about 50 Å in diameter under H<sub>2</sub>, CO and H<sub>2</sub>O (and mixtures thereof)<sup>9</sup>.

The most precise observations of sintering (though not redispersion) have been made in model supported-Pd systems, using scanning tunnelling microscopy<sup>10–14</sup>. However, though elegant, this approach currently lacks the time resolution to see 'inside' all but rather slow processes. It also requires the use of planar model systems generally (though not always<sup>10</sup>) maintained in an ultrahigh-vacuum environment, rather than catalysts operating under more realistic conditions. In the world of auto-exhaust catalysis, this can mean situations wherein the redox potential of the feedstock can change very rapidly indeed (between, for instance, feedstocks containing differing levels of CO and NO: so-called 'Lambda' cycling)<sup>15</sup>. Nonetheless, scanning tunnelling microscopy has shown *in vacuo* sintering by an Ostwald ripening mechanism of Pd particles commencing above 700 K (refs 12,13), CO-induced Pd mobility and sintering on planar SiO<sub>2</sub> substrates<sup>11</sup>, two routes to CO oxidation based on metallic and oxidic Pd (ref. 10) and that Pd nanoparticle oxidation can exhibit a significant size dependence<sup>14</sup>. Furthermore, recent density functional theory calculations<sup>16</sup> concerning very small (Pd<sub>4</sub>–Pd<sub>9</sub>) Pd clusters supported on MgO have indicated that a low-temperature route to oxidation in O<sub>2</sub> may be possible. However, so far direct and real-time *in situ* observation of sintering and redispersion has not been achieved. Therefore, the detailed structural-dynamic information that could provide the basis for fully understanding these phenomena and, as a result, controlling them for practical application, has evaded elucidation.

We have synchronously applied energy-dispersive extended X-ray absorption fine-structure (EXAFS) spectroscopy, diffuse reflectance infrared spectroscopy (DRIFTS) and mass spectrometry

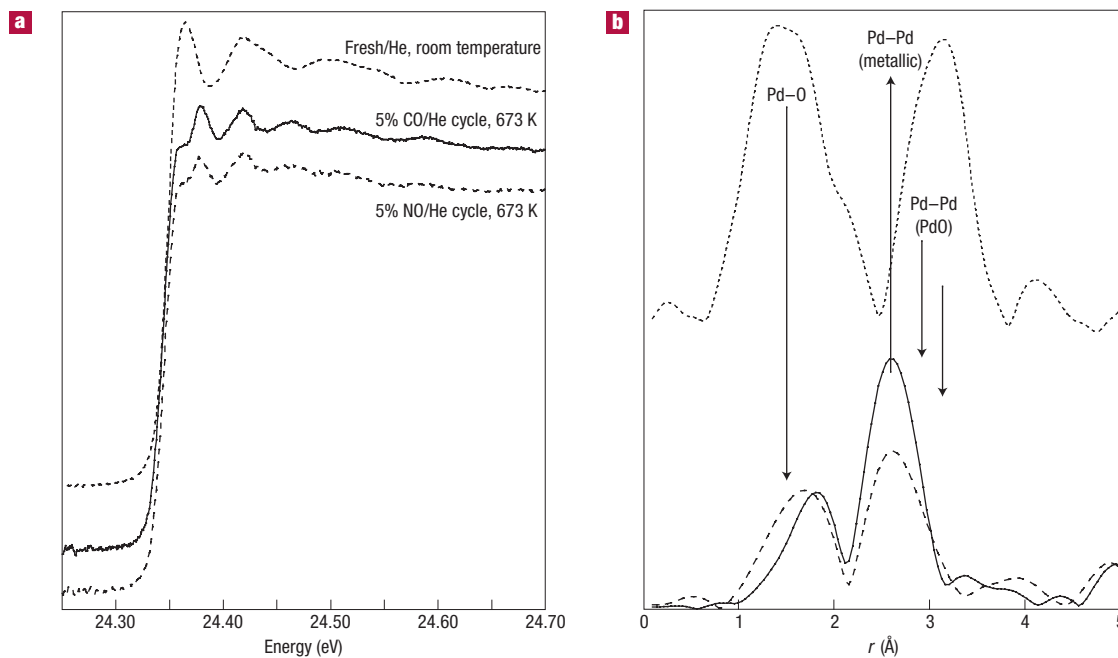


**Figure 1** Raw absorption and Fourier-transform representation of Pd K-edge dispersive EXAFS data in three different situations. **a**, Background-subtracted Pd K-edge dispersive EXAFS data derived from 1 wt% Pd/10ZCA in three situations. The edge jump = 0.3. Acquisition times are: fresh = 1,000 ms; during CO/NO cycling at 673 K = 250 ms. **b**,  $k^3$ -weighted Fourier-transform representation of the data shown in **a**. Top spectrum (dotted line) = ‘fresh’ 1 wt% Pd/10ZCA sample at room temperature. The solid black line was obtained at the end of a CO cycle ( $t = 131$  s, Fig. 2); the dashed line was obtained at the end a NO cycle ( $t = 113$  s, Fig. 2).

to investigate the structural reactive behaviour of a 1% Pd in 10ZCA (Pd/10ZCA) catalyst cycling between flows of 5% CO/He and 5% NO/He at 673 K. EXAFS spectroscopy is a direct probe of local structure and is best applied when the domain size of the objects under study is very small<sup>17</sup> as is often found in precious-metal catalysts. EXAFS spectroscopy therefore provides a structural window, where diffraction and microscopy (for example, TEM) are becoming less effective as a result of these reduced domain dimensions, typically below 20 Å. In addition, in the latter case, heavy elements such as Ce and Zr in the support material (as in the system under study here) lead to increasingly limiting contrast issues. Furthermore, when applied in dispersive mode, EXAFS spectroscopy has the potential for a high time resolution in a single measurement<sup>18</sup>. DRIFTS permits interrogation of the nature of the adsorbates present on the surface of the catalyst together with the formation or consumption of certain gas-phase species; similarly to dispersive EXAFS spectroscopy it can be applied with high time resolution. Mass spectrometry provides a measure of the global catalytic process that occurs by monitoring the composition of the gaseous feedstock. Therefore, in this experiment, we have the tools to study processes *in situ*, from local (surface and bulk) structure, functional and reactivity viewpoints, simultaneously, and with a subsecond time resolution (3–4 Hz in the current instance).

Here, we concentrate on the nature and rapidity of transformations of the Pd phase occurring during CO/NO cycling and catalytic reduction of NO by CO. We show the existence of a novel and rapid redispersion mechanism that occurs without significant oxidation of the Pd phase and in the absence of Cl. Moreover, from the combination of techniques applied simultaneously, we are able to understand the fundamental origins of this novel behaviour and how they act together to yield effective NO reduction and CO removal. In addition, this approach

should be more generally applicable to understanding a range of phenomena of central importance to the performance of catalysts and other functional materials in a variety of areas.

Figure 1 shows dispersive EXAFS data in (1) a background-subtracted absorption form and (2) a Fourier-transform representation. The expected positions within the Fourier transform of a variety of Pd–X (X = O, Pd) coordinations are indicated. A summary of the structural and statistical data derived from analysis of the spectra shown (along with those derived from the post-reaction system at both 673 and 300 K) is given as Supplementary Information.

As expected<sup>19,20</sup>, the fresh catalyst (see Fig. 1a) comprises nanoparticulate PdO. In this case, therefore, the X-ray absorption near-edge structure (XANES) indexes 100% Pd<sup>2+</sup>. However, the two cases taken from within the CO/NO oscillation experiment at 673 K show that, irrespective of the environment (5% NO/He or 5% CO/He), the Pd–Pd bond length is that expected from nanoparticulate and metallic Pd ( $r_{\text{Pd–Pd}} \sim 2.71$  Å), with little evidence for a PdO-type phase. Under CO, it can be seen that the Pd–Pd coordination is augmented compared with the situation found under NO (see the Supplementary Information).

At first sight, these variations in coordination number could be associated with the commonly encountered oxidation and reduction of the supported particles<sup>21,22</sup>. Within this scenario, the fast changes observed would relate to the oxidation of a thin outer layer of the particles. This would then be followed by a slower permeation of the nascent oxide phase throughout the particles. However, if simple oxidation, rather than changes in the size and/or shape of the metallic Pd particles, were the predominant cause of these observations, we would need to invoke a  $\geq 50\%$  conversion of Pd<sup>0</sup> to Pd<sup>2+</sup> to accompany a change in Pd coordination of 8 to between 5 and 6 (ref. 17). Such a change should be clearly visible in the XANES, which is quantitatively diagnostic<sup>19–21</sup> in this

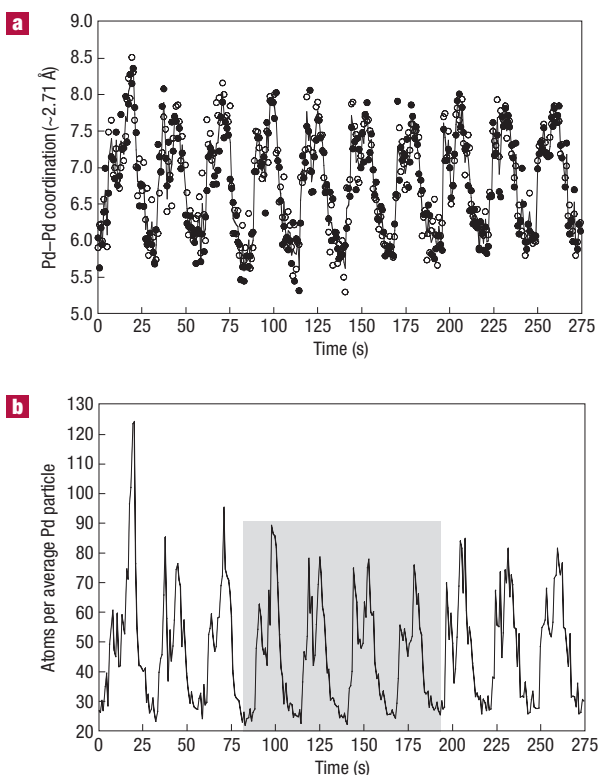


**Figure 2** Relating Pd–Pd coordination number and the apparent number of atoms per Pd particle during CO/NO cycling. **a**, The coordination data from the first (solid circles) and second (open circles) successive cycling experiments; the solid line is the average of the two. Each point corresponds to a single, 250 ms, EXAFS spectrum. **b**, Temporal variation in the apparent average number of atoms per Pd nanoparticles during CO/NO cycling at 673 K over a 1 wt% Pd/10ZCA sample derived from the Pd–Pd coordination numbers extracted from EXAFS data. The highlighted grey area is shown in more detail in Fig. 3.

sense (see Fig. 1 and Supplementary Information). As this is not observed, simple oxidation can be eliminated as the dominant process at work here. This is not to say that there is a total absence of oxidation to Pd<sup>2+</sup>. Both the EXAFS and (in particular) the XANES data do yield evidence of a subsidiary role for this process but place an upper limit of only about 10% Pd oxidation to Pd<sup>2+</sup> at any point in the experiment (see the Supplementary Information).

This being the case, we must invoke a different type of structural change to explain these results. In the simplest approximation (that assumes an invariant particle morphology), the coordination number changes would indicate that Pd particles of up to around 100 atoms, initially sintered by CO, can be very rapidly, reversibly, and essentially non-oxidatively, dispersed by NO to yield particles of about 20–25 atoms. It is this simplest view that is shown in Fig. 2, where the temporal variation of the Pd–Pd ( $r_{\text{Pd-Pd}} \sim 2.71 \text{ \AA}$ ) coordination number (shown in Fig. 2a for two successive cycling experiments at 673 K) is interpreted in terms of the number of atoms present in the average Pd particle<sup>17</sup>. Alternatively, such coordination number variation could also arise from morphological change (that is, a flattening and unflattening of Pd particles whilst retaining a constant particle volume). Both situations are the potential interpretation extremes, with a combination being the most likely.

Although, hypothetically, EXAFS spectroscopy has the potential to discriminate between these two possibilities, this requires the

quantification of the relative occupancies of shells beyond the first<sup>17</sup>. Furthermore, for this type of ‘shape’ analysis to be reliable, the appropriate disorder parameters for each shell need to be known; unfortunately, this is rarely ever the case. In this respect, therefore, we can go no further, except for stating that one or both of these possibilities is at work in this system. However, the data obtained do allow us to estimate some limits for each possibility. The variation of coordination numbers indicates, within the approximations used<sup>17</sup>, that particles of an average of  $\sim 80$  atoms reversibly disintegrate into entities of about 20 atoms. If we assume a constant (hemispherical) morphology throughout, this translates into an average particle of  $\sim 7.5 \text{ \AA}$  radius (under CO) splitting into four particles of about  $4.7 \text{ \AA}$  radius under NO. Within this constant morphology paradigm, the particle dispersion and particle–oxide interfacial area increase by  $\sim 60\%$ . Concomitant with this is a factor 2.5 increase in the total Pd–oxide perimeter. If we assume a constant particle volume (flattening) scenario, then to achieve the same net increase in metal–oxide interface area, a disc of  $\sim 9.5 \text{ \AA} \times 3.1 \text{ \AA}$  would result (roughly a Pd bilayer raft); in this case, the total Pd particle dispersion increases by about 33% and the perimeter increases by about 25%. Therefore, both possibilities, as indicated by the EXAFS data, would seem at least structurally feasible from this simple point of view. Further CO adsorption experiments carried out after the CO/NO cycles indicate that, in fact, both size and shape changes occur here (see the Supplementary Information).

Figure 3 takes the highlighted area shown in Fig. 2 and, alongside the data derived from the EXAFS spectra, incorporates the behaviour of species observed in the DRIFTS component of the experiment, namely: CO<sub>2(g)</sub> ( $2,356 \text{ cm}^{-1}$ ), adsorbed NCO species ( $2,242 \text{ cm}^{-1}$ ), bridging (a CO species shared by two Pd atoms) and threefold (a CO species shared by three Pd atoms) CO species adsorbed on Pd ( $1,925 \text{ cm}^{-1}$ ) and carbonate species partially associated with the CeZr phase of the support ( $1,379/1,556 \text{ cm}^{-1}$ ) (refs 19,20). It should be noted that other Pd<sup>0</sup>–CO species (threefold/bridged, at  $1,864 \text{ cm}^{-1}$  and linear, atop (a CO attached to one Pd atom), at  $2,048 \text{ cm}^{-1}$ ) are also observed to show the same temporal behaviour. Figure 4 schematically shows the most salient information derived from the experiment (see also Supplementary Information). At the start of the reducing (CO) cycle (point A, Figs 3 and 4) the Pd exists as dispersed or flattened (quasi-two-dimensional) particles with partially oxidized surfaces. This adsorbed oxygen is rapidly removed as CO<sub>2</sub> (Figs 3 and 4). Within this first phase of CO<sub>2</sub> production, it is also clear that contributions also arise from carbonate species ( $1,379 \text{ cm}^{-1}$  and  $1,556 \text{ cm}^{-1}$ ) that may exist adsorbed on the CeZr and Al<sub>2</sub>O<sub>3</sub> phases of the support. As this phase of CO<sub>2</sub> production reaches completion, the EXAFS data indicate that the Pd sinters or takes on a more three-dimensional habit. Infrared bands indicative of atop ( $2,050 \text{ cm}^{-1}$ ) and bridging/threefold ( $1,925$  and  $1,864 \text{ cm}^{-1}$ ) CO adsorbed on metallic Pd (point B, Figs 3 and 4) can be observed concurrently. These only appear after the oxygen has been removed from the Pd or Pd–Ce interface and do not have any relation to this first phase of CO<sub>2</sub> production. Here we note that, although we have made great progress in understanding the behaviour of this system, the reproducible dip (not concurrently observed in the infrared from the CO forming on the Pd nanoparticles) in the apparent average number of atoms of the Pd particles during the CO cycle is one aspect that remains to be fully comprehended.

On switching to the NO feed, the CO species adsorbed on the Pd are very abruptly removed and redispersion via particle splitting or flattening occurs (point C, Figs 3 and 4). The second stage of CO<sub>2</sub> production now observed would normally correspond to, in the terminology of Hendriksen *et al.*<sup>10</sup>, the ‘metallic branch’ of CO oxidation. However, close inspection of the appearance and

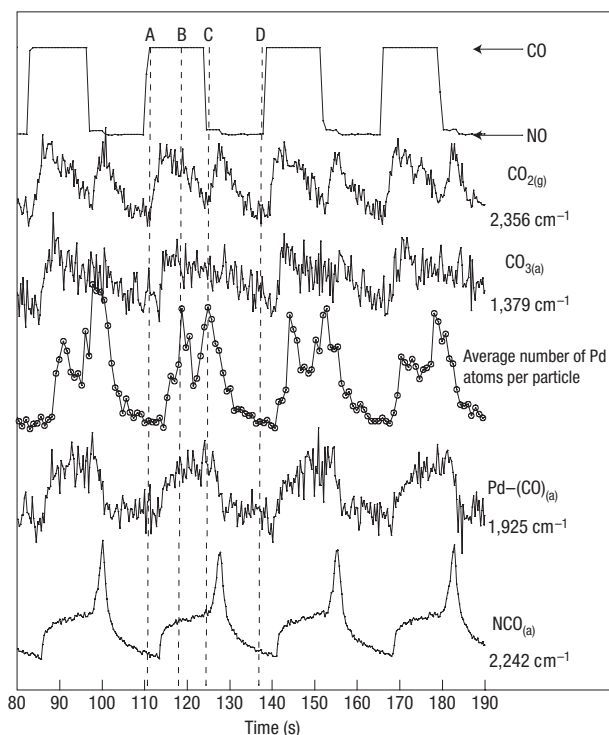


**Figure 3** Correlating structural changes with temporal variations of infrared active adsorbates and  $\text{CO}_2$  evolution during CO/NO cycling. Collation of the average number of atoms of the Pd particles (open circles) with the concurrently observed temporal responses in DRIFTS for: adsorbed carbonate species ( $1,379\text{ cm}^{-1}$ ); gas phase  $\text{CO}_2$  ( $2,356\text{ cm}^{-1}$ ); bridge bonded CO and threefold CO adsorbed on Pd ( $1,925\text{ cm}^{-1}$ ); and from adsorbed NCO species ( $2,242\text{ cm}^{-1}$ ). The changes in feedstock composition are indicated at the top of the graph. The points A–D refer to those points indicated in Fig. 4 and in the text. The different data are offset for clarity. (a) and (g) refer to adsorbed and gaseous, respectively.

disappearance of  $\text{CO}_2$  and the surface Pd(CO) species (Fig. 3) indicates a different time evolution; the  $\text{CO}_{2(\text{g})}$  signal rises before, and falls considerably after, removal of the adsorbed CO.

The measurement of the turnover frequency in similar experimental conditions (CO, NO pulse experiments, 673 K; Pd nanoclusters below  $15\text{ \AA}$ ) gives values below  $10^{-1}$  molecules  $\text{s}^{-1}$  for  $\text{CO}_2$  production<sup>23</sup>, indicating that the corresponding surface precursor species could be visible using our subsecond time resolution and must correlate with the  $\text{CO}_{2(\text{g})}$  signal. Under this framework of thinking, the synchronous DRIFTS should be able to give some clues that contribute to resolving this conundrum. It shows that there are species that bridge the gap between the rapid removal of Pd<sup>0</sup>(CO) functionality, the production of  $\text{CO}_2$  and the non-oxidative redispersion of the Pd: adsorbed NCO species. NCO species could provide an effective sink for the O atom released through NO dissociation<sup>24</sup>, accounting significantly, alongside simple desorption, for the rapid removal of Pd(CO), and evolving, by subsequent decomposition, as  $\text{N}_2$  and  $\text{CO}_2$ ; hence the observed rapid formation then disappearance of the NCO band concomitant with  $\text{CO}_{2(\text{g})}$  production (Fig. 3; between points C and D).

To summarize, using an *in situ* dispersive EXAFS spectroscopy/DRIFTS/mass spectrometry approach we have revealed that very rapid, reversible sintering and novel, non-oxidative redispersion phenomena can readily be observed in

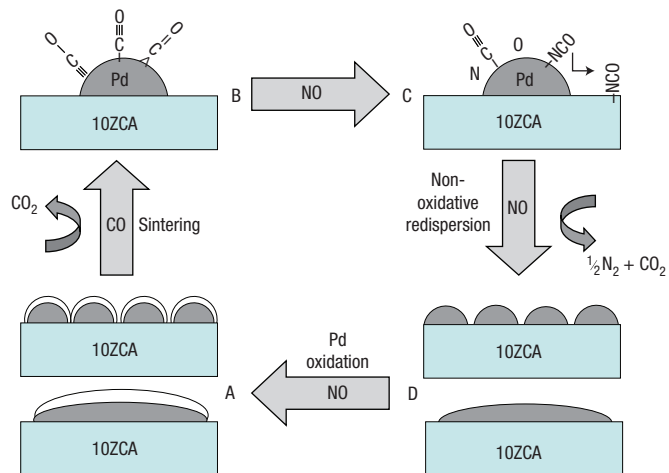


**Figure 4** A schematic representation of the fundamental steps underlying the reversible, non-oxidative, size (redispersion and sintering) and/or shape changes of Pd nanoparticles during CO/NO cycling. Points A–D mark the most salient positions within a CO/NO cycle as indicated in Fig. 3 and in the text.

supported 1 wt% Pd catalyst systems during CO/NO cycling at 673 K. Whether this sintering and redispersion behaviour involves absolute changes in size or gross morphological variation (or indeed both) remains to be definitively determined. Nonetheless, we are able to clearly differentiate these processes from the more simple oxidation and reduction of the Pd nanoparticles and show that this structural change forms an integral part of the CO/NO deNO<sub>x</sub> cycle over Pd. A pivotal role of the intermediary NCO species is suggested by the present results. The overall importance of this novel, and notionally  $\text{N}_2\text{O}$  free, redispersion/sintering cycle to deNO<sub>x</sub> processes will, however, clearly be determined by how it competes with, for instance, oxidation of the metal phase. The available evidence for Rh-based systems shows that oxidation (by NO and  $\text{O}_2$ ) is very fast<sup>22,25,26</sup> at comparable temperatures, and may therefore dominate, or at least compete, in similar situations. For Pd, Pt and other less oxophilic metals, how such a process might compete with oxidation of the metal is far less clear. However, this method now provides a means to fully explore, and parameterize, processes such as this and the extent of their importance in progressively more realistic situations.

## METHODS

The experimental set-up used is a development of that published previously<sup>25,26</sup>. The 1 wt% Pd on 10 wt% ceria–zirconia on alumina (1Pd/ZCA) samples were synthesized as described previously<sup>19–21</sup>. About 40–50 mg of sample, sieved to a 112–80  $\mu\text{m}$  fraction, was used per experiment.

Experiments were carried out on ID24 at the ESRF. EDE measurements were carried out using a Si (311) polychromator in the Bragg configuration and a 16-bit FReLoN detector<sup>22,25,26</sup>. Methods for optimizing the EXAFS data from these types of sample<sup>27</sup> were also implemented so that dispersive EXAFS data of such dilute Pd samples could be obtained. Data reduction and analysis of the EXAFS data was carried out using PAXAS (PAXAS: Programme for the analysis of X-ray adsorption spectra, University of Southampton (1988)) and EXCURV (N. Binsted, EXCURV, CCLRC Daresbury Laboratory Computer Programme (1998)).

DRIFTS measurements were recorded using a Bruker IFS 66 spectrometer and a high-sensitivity mercury–cadmium–telluride detector. Samples were heated under a flow of He to 673 K and then subjected to cycles comprising alternate (CO first) flows (2 bar,  $75\text{ ml min}^{-1}$ ) of 5% CO/He (13.8 s) and 5%

NO/He (13.8 s) whilst dispersive EXAFS, DRIFTS and mass spectrometry data were collected synchronously. After finishing the cycle with an exposure to NO, the flow was returned to He and the experiment was repeated at 673 K before cooling under He to 300 K. Adsorption experiments of CO at room temperature after the CO and NO cycles were also carried out by allowing contact with He at 673 K for 5 min and cooling in the same gas at room temperature. A 5% CO/He stream (30 ml min<sup>-1</sup>; 5 min) and a subsequent purge in He were used to obtain the spectra after each step.

Received 15 December 2006; accepted 12 April 2007; published 27 May 2007.

## References

- Dalla Betta, R. A., McCune, R. C. & Sprys, J. W. Relative importance of thermal and chemical deactivation of noble metal automotive oxidation catalysts. *Ind. Eng. Chem. Prod. Res. Dev.* **15**, 169–172 (1976).
- Che, M. & Bennett, C. O. The influence of particle size on the catalytic properties of supported metals. *Adv. Catal.* **36**, 55–172 (1989).
- Leiske, H., Lietz, G., Spindler, H. & Volter, J. Reactions of platinum in oxygen treated and hydrogen treated Pt- $\gamma$ -Al<sub>2</sub>O<sub>3</sub> catalysts 1. Temperature programmed reduction, adsorption and redispersion of platinum. *J. Catal.* **81**, 8–16 (1983).
- Leiske, H., Lietz, G., Spindler, H., Hanke, W. & Volter, J. Reactions of Platinum in oxygen treated and hydrogen treated Pt- $\gamma$ -Al<sub>2</sub>O<sub>3</sub> catalysts 2. Ultraviolet visible studies, sintering of platinum, and soluble platinum. *J. Catal.* **81**, 17–25 (1983).
- Birgersson, H., Eriksson, L., Boutonnet, M. & Jaras, S.G. Thermal gas treatment to regenerate spent automotive three-way exhaust catalysts (TWC). *Appl. Catal. B* **54**, 193–200 (2004).
- Cabello-Galisteo, et al. Reactivation of sintered Pt/Al<sub>2</sub>O<sub>3</sub> oxidation catalysts. *Appl. Catal. B* **59**, 227–223 (2005).
- Daley, R. A., Christou, S. Y., Efstathiou, A. M. & Anderson, J. A. Influence of oxychlorination treatments on the redox and oxygen storage and release properties of thermally aged Pd–Rh/Ce<sub>2</sub>Zr<sub>1-x</sub>O<sub>2</sub>/Al<sub>2</sub>O<sub>3</sub> model three-way catalysts. *Appl. Catal. B* **60**, 2117–227 (2005).
- Harris, P. J. E. Sulphur-induced faceting of platinum catalyst particles. *Nature* **323**, 792–794 (1986).
- Hansen, P. L. et al. Atomic resolved imaging of dynamic shape changes in supported copper nanocrystals. *Science* **205**, 2053–2055 (2002).
- Hendriksen, B. L. M., Bobaru, S. S. & Frenken, J. W. M. Oscillatory CO oxidation on Pd(100) studied with in situ scanning tunneling microscopy. *Surf. Sci.* **552**, 229–242 (2004).
- Lu, J.-L. et al. Low temperature CO induced growth of Pd supported on a monolayer silica film. *Surf. Sci. Lett.* **600**, L153–L157 (2006).
- Howard, A., Mitchell, C. E. J. & Edgel, R. E. Real time STM observation of Ostwald ripening of Pd nanoparticles on TiO<sub>2</sub>(110) at elevated temperatures. *Surf. Sci. Lett.* **515**, L504–508 (2002).
- Stone, P., Poulston, S., Bennett, R. A. & Bowker, M. Scanning tunnelling microscopy investigation of sintering in a model supported catalyst: nanoscale Pd on TiO<sub>2</sub>(110). *Chem. Commun.* 1369–1370 (1998).
- Schalow, T. et al. Size-dependent oxidation mechanism of supported Pd nanoparticles. *Ange. Chem. Int. Edn.* **45**, 3693–3697 (2006).
- Farrauto, R. J. & Heck, R. M. Catalytic converters: State of the art and perspectives. *Catal. Today* **51**, 351–360 (1999).
- Huber, B., Kosinen, P., Hakkinen, H. & Moseler, M. Oxidation of magnesia-supported Pd-clusters leads to the ultimate limit of epitaxy with a catalytic function. *Nature Mater.* **5**, 44–47 (2006).
- Jentys, A. Estimation of mean size and shape of small metal particles by EXAFS. *Phys. Chem. Chem. Phys.* **1**, 4059–4063 (1999).
- Newton, M. A., Dent, A. J. & Evans, J. Bringing time resolution to EXAFS: Recent developments and application to chemical systems. *Chem. Soc. Rev.* **31**, 83–95 (2002).
- Fernandez-Garcia, M. et al. New Pd/Ce<sub>2</sub>Zr<sub>1-x</sub>O<sub>2</sub>/Al<sub>2</sub>O<sub>3</sub> three-way catalysts prepared by microemulsion—Part 1. Characterization and catalytic behaviour for CO oxidation. *Appl. Catal. B* **31**, 39–50 (2001).
- Martinez-Arias, A. et al. New Pd/Ce<sub>2</sub>Zr<sub>1-x</sub>O<sub>2</sub>/Al<sub>2</sub>O<sub>3</sub> three-way catalysts prepared by microemulsion—Part 2. In situ analysis of CO oxidation and NO reduction, under stoichiometric CO+NO+O<sub>2</sub>. *Appl. Catal. B* **31**, 51–60 (2001).
- Iglesias-Juez, A., Martinez-Arias, A., Newton, M. A., Fiddy, S. G. & Fernández-García, M. Redox behaviour of Pd-based TWCs under dynamic conditions: Analysis using dispersive XAS and mass spectrometry. *Chem. Commun.* 4092–4094 (2005).
- Newton, M. A., Fiddy, S. G., Guilera, G., Jyoti, B. & Evans, J. Oxidation/reduction kinetics of supported Rh/Rh<sub>2</sub>O<sub>3</sub> nanoparticles under plug flow conditions using dispersive EXAFS. *Chem. Commun.* 118–119 (2005).
- Heiz, U. & Bullock, E. L. Fundamental aspects of catalysis on supported metal clusters. *J. Mater. Chem.* **14**, 564–577 (2004).
- Solymosi, F. & Banasagi, T. On the participation of NCO surface species in the NO+CO reaction. *J. Catal.* **202**, 205–206 (2001).
- Newton, M. A., Dent, A. J., Fiddy, S. G., Jyoti, B. & Evans, J. Combining diffuse reflectance spectroscopy (DRIFTS), dispersive EXAFS, and mass spectrometry with high time resolution: potential, limitations, and application to the study of the interaction of NO with supported Rh catalysts. *Catal. Today* (2006) (doi:10.1016/j.cattod.2006.09.034).
- Newton, M. A., Dent, A. J., Fiddy, S. G., Jyoti, B. & Evans, J. Identification of the surface species responsible for N<sub>2</sub>O formation from the chemisorption of NO on Rh/alumina. *Phys. Chem. Chem. Phys.* **9**, 246–249 (2007).
- Newton, M. A. Beamsize related phenomena and effective normalisation in energy dispersive EXAFS for the study of heterogeneous catalysts, powder materials, and the processes they mediate: Observations, and (some) solutions. *J. Synchrotron Rad.* (in the press).

## Acknowledgements

The authors would like to thank the ESRF for access to facilities and for the funding that permitted the development of this experiment on ID24. T. Mairs, F. Perrin, G. Guilera and A. Kroner are thanked for the various contributions they have made to this work; S. Pascarelli and O. Mathon are thanked for their general support and stewardship of the beamline. Finally, we acknowledge the CYCIT (projects CTQ2004-03409/BQU and CTQ2006-15600/BQU) for financial support. C. Belver thanks the Spanish 'Ministerio de Educación y Ciencia' for a 'Juan de la Cierva' postdoctoral grant. Correspondence and requests for materials should be addressed to M.A.N. or M.F.-G. Supplementary Information accompanies this paper on [www.nature.com/naturematerials](http://www.nature.com/naturematerials).

## Competing financial interests

The authors declare no competing financial interests.

Reprints and permission information is available online at <http://npg.nature.com/reprintsandpermissions/>